Analyst

Accepted Manuscript

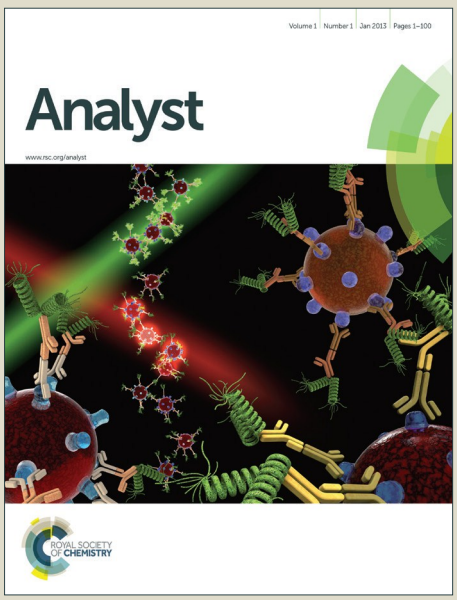

ROYAL SOCIETY OF CHEMISTRY

www.rsc.org/analyst

Analyst

RSCPublishing

ARTICLE

High throughput absorbance spectra of cancerous cells: a microscopic investigation of spectral artifacts

Cite this: DOI: 10.1039/x0xx00000x

A. Mignolet[a] and E. Goormaghtigh[a,*]

Received ooth January 2012,
Accepted ooth January 2012

DOI: 10.1039/x0xx00000x

www.rsc.org/

FTIR spectroscopy was recently demonstrated to be a useful tool to obtain a unique fingerprint of the effects of several anticancer drugs on cells in culture. While FTIR spectroscopy appears to have a definite potential to sort anticancer drugs on the basis of the metabolic modifications they induced, the present challenge remains to evaluate the drug-induced spectral changes in cancer cells on a larger scale. Coupling FTIR spectroscopy with a high throughput screening extension could become a useful tool to generate drug classifications based on their "modes of action". Practically, the robustness of this approach is jeopardized by the variability that can appear from one cell smear to the next. Scattered cells result in strong scattering effects and locally dense cell aggregates could result in non-linearity of the signal. A microscopic study using infrared imaging demonstrates that the mean HTS (96-well High Throughput Spectroscopy) spectra recorded on 96 well ZnSe plates are the average of contributions characterized by a wide absorbance distribution and by Mie scattering effects which significantly vary from point to point. Spectrum quality is the best at the highest cell concentrations, i.e. 300,000 to 400,000 cells/well which presents the best S/N and the relatively smaller Mie scattering effect. When the breast cancer cell line MDA-MB-231 was treated with four different polyphenols, spectra showed quite similar variations with respect to control spectra with more intense variations for the quercetin and EGCG compared to resveratrol and capsaicin. Correction of the spectra with the RMieS algorithm improved their clustering according to the polyphenolic treatment.

Introduction

The number of anticancer agents that fail in the clinic far outweighs those considered effective, suggesting that the selection procedure for progression of drug molecules into the clinic requires improvement. Traditionally new drugs are evaluated for their potential to inhibit the proliferation of cancer cell lines[1] (e.g. IC_{50} measurements) but this approach may not be sufficient anymore to identify new drugs. It also fails to reveal potential interesting leads with innovative modes of action if the IC_{50} is too high as the molecule will be immediately discarded.

Infrared spectroscopy is sensitive to all molecules (proteins, lipids, sugars, etc.) present in cells but, importantly, it is also sensitive to molecular details such as protein conformation[2–6] or lipid nature, chain length and unsaturation level.[7,8] In turns, spectra of cells depend on cell cycle,[9–15] confluence stage,[16] cell strain[17] and interestingly on the various metabolism perturbations induced by potential anticancer drugs such as gemcitabine,[18] platinum derivatives,[19] cardiotonic steroids[20–23] and polyphenols.[24], allowing some level of "modes of action" to be identified.[21–23,25–27] As this spectral technique can offer a global insight in the biological and physiological processes mediated by a drug, it can be useful to follow the effects of a large panel of new molecules. Unlike conventional techniques used in cellular or molecular biology, infrared spectroscopy yields a precise image of all the chemical bonds present in the sample and offers the opportunity to observe very quickly all metabolic modifications induced by a drug. Therefore the action on different drug targets is likely to yield different infrared fingerprints characteristic of the "mode of action" of the therapeutic agent under investigation. In turn, drug-induced metabolic disorders should be amenable to classification in the same way bacteria gender, species, and strains can be classified.[28–31] For example, after the treatment of PC-3 prostate cancer cells with 7 anticancer drugs used in the clinics, FTIR could classify them in 3 groups corresponding to 3 well-known anti-cancerous mechanisms of action.[25] More recently, clustering by mechanism of action was extended to 6 other cell lines using 4 anticancer drugs and was found to be similar for all cell lines.[26]

While FTIR spectroscopy appears to have a definite potential to sort anticancer drugs on the basis of the metabolic modifications they induced, the present challenge remains to evaluate drug-induced spectral changes in cancer cells on a larger scale. In traditional approaches, the possibility of testing a large number of synthetic or natural compounds in a short

period of time by high throughput screening (HTS) has gained widespread popularity over the last two decades. It has become a standard method for drug discovery in the pharmaceutical industry[32] as the ability to test large numbers of compounds quickly and efficiently can provide a competitive advantage that makes HTS a key tool for many companies.[33] Therefore the coupling of FTIR spectroscopy with a high throughput screening extension could become a useful tool to generate drug classifications based on "modes of action". Practically, the robustness of this approach has been jeopardized by the variability that can appear from one cell smear to the next one. This variability has been largely solved by replacing a single deposit by a robotic deposition of hundreds of spots of 200 pl each in each well.[34] This robotics automation minimizes the user interactions with the sample to get more reproducible and homogeneous procedure but it requires the use of a multi-spotter and slows down the process. In the present paper we address the question of the best experimental conditions when a robot is not used.

Materials and Methods

Cell culture

Three human mammary breast cancer cell lines (MDA-MB-231, MCF-7 and SK-BR-3) were acquired from the American Type Culture Collection (ATCC, Manassas, VA) and were maintained according to the supplier's instructions. A fourth one, the HBL-100 cell line, was received from the department of toxicology of the Université Libre de Bruxelles. This cell line was cultivated in the same conditions as the three other breast cancer cell lines. The cells were grown in a constant humidified atmosphere of 5% CO_2 in air and were kept in exponential growth in RPMI medium supplemented with 10% foetal bovine serum (FBS), 2% penicillin/streptomycin (an antibiotic solution) and 1% L-glutamine. Cell culture medium, and antibiotics were purchased from Lonza (Verviers, Belgium) and the FBS from Life Technologies (California, USA). Cultures were tested twice a month for mycoplasma infections using PlasmoTest from InvivoGen (Toulouse, France).

FTIR spectroscopy/imaging

Cell handling

For FTIR spectroscopy, cells were grown to sub-confluence i.e. ca. 80 % of confluence as defined elsewhere.[16] Cells were then detached from their culture support by means of a five-minute treatment with trypsin at 37°C (0.5 g/l) / EDTA 0.2 g/l buffer (Lonza, Verviers, Belgium). The reaction was stopped by adding culture medium. The cells were collected and counted using a Neubauer cell to prepare 15 ml falcons with different quantities of cells to be deposited on the plate. For each count, the quantity of cells collected was tripled to allow a triplicate within the experience. The cells were then pelleted by a 7-minute centrifugation (230 g) and washed three times in isotonic solution (NaCl, 0.9%) to ensure complete removal of trypsin and culture medium that absorb in the infrared region of interest. The different cell pellets were re-suspended in about 30 µl isotonic solution and 10 µl were deposited on each well of the ZnSe 96-well plate designed for HTS-FTIR analysis (Bruker). Cell count varied from 50,000 to 400,000 cells per well. Once all the samples were deposited on the plate, it was placed at 37°C in an incubator during 1 hour to dry.

Infrared measurements

The IR data were recorded using a high throughput screening extension (HTS-XT) connected to a Bruker FTIR Tensor27 spectrometer. The microplate extension HTS-XT allows the recording of infrared spectra of 96 samples in an automated manner. The infrared spectra were acquired in transmission mode between 4000 and 400 cm^{-1} at a resolution of 2 cm^{-1}. The spectrometer was equipped with DLaTGS detector. The diameter of the IR beam is around 6 mm and so, the infrared spectrum recorded for one well of the ZnSe 96-well plate represents the composition of the entire well. It took about 4 hours to record the infrared spectra of 72 wells. 128 scans were averaged for each spectrum.

For infrared imaging, the infrared spectra of the same samples were collected using a Hyperion 3000 IR imaging system (Bruker Optics, Ettlingen, Germany), equipped with a liquid N_2 cooled 64*64 Mercury Cadmium Telluride (MCT) Focal Plane Array (FPA) detector. Both the microscope and the sample compartment were constantly purged with dry air. The data were collected in transmission mode. 64×64 pixels were recorded at a magnification of 15 X on a 2560 × 2560 µm² detector. In turn, the size of the image was 180 × 180 µm² and the pixel size was 2.8*2.8 μm^2. Yet, if the effective pixel size defines the best possible spatial resolution, the actual spatial resolution is decreased by in-between pixel blurring related to the IR wavelength as discussed later. It took about 16 minutes to record an FTIR image of 16384 spectra (4 units image) at 256 scans and 8 cm^{-1}.

Data analyses

Pre-processing. All infrared data were preprocessed as follows. For HTS-spectra, water vapor contribution was subtracted after adjusting subtraction coefficients and shifts of several water vapor spectra by a minimization procedure described elsewhere.[35,36] The CO_2 peak was flattened between 2450 and 2250 cm^{-1}. In the case of FTIR images, the water vapor contribution was subtracted as described previously [35,37] with 1956-1935 cm^{-1} as reference peak. The CO_2 peak was flattened between 2450 and 2250 cm^{-1}. The signal to noise ratio (S/N) was then systematically checked on every spectrum. For HTS spectra, this ratio was required to be greater than 300 when noise was defined as the standard deviation in the 2000-1900 cm^{-1} region of the spectrum and the signal, the maximum of the curve between 1750 and 1480 cm^{-1} after a baseline passing through these two points had been subtracted. For FTIR images, this ratio was fixed at 100.

Correction of the spectra for water vapor contribution, baseline subtraction, normalization, Student t-test and principal component analyses were all carried out by Kinetics, a custom made program running under Matlab (Matlab, Mathworks Inc). The RMies-EMSC algorithm used to correct the spectra for Resonant Mie Scattering was written by Bassan et al.[38] and also runs under Matlab.

Results and discussion

High throughput infrared spectra at various cell densities

To evaluate the best conditions to record FTIR spectra of cells deposited on a ZnSe 96-well plate, the number of cells was varied from 50,000 to 400,000 per well. To avoid formation of cell multilayers, no more than 400,000 cells were deposited on the wells in this work. Figure 1 illustrates a cell smear of 200,000 MDA-MB-231 cells deposited to form a spot

of about 6 mm of diameter. The image shows that the cell smear is rather homogenous in its center, the outer region appears to be less concentrated.

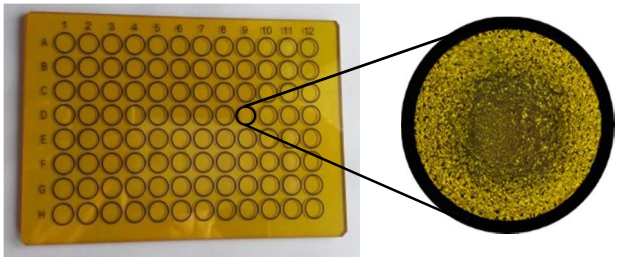

***Figure 1**; a 96-well ZnSe plate with a enlargement of one well containing 200,000 MDA-MB-231 cells.*

Figure 2 presents HTS-FTIR spectra recorded for the different amounts of MDA-MB-231 cells deposited on a HTS plate well. As expected, the absorbance increases as the number of cells increases. At the same time, the S/N increases linearly with the absorbance (not shown).

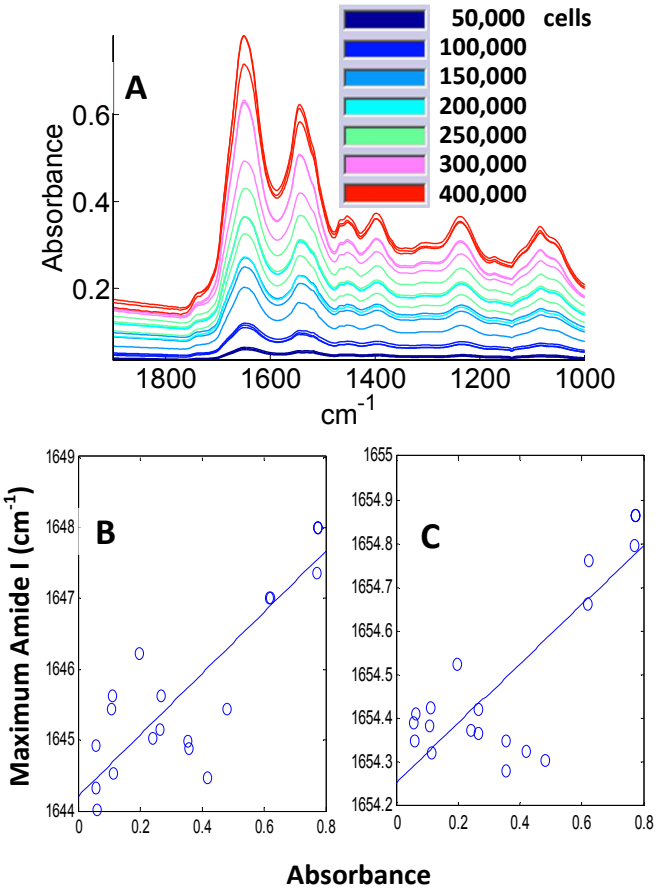

***Figure 2**: A. Series of HTS-FTIR spectra of MDA-MB-231 cells for 50,000 - 100,000 – 150,000 – 200,000 – 250,000 – 300,000 and 400,000 cells deposited on HTS plate wells. Only water vapor has been corrected as described in Methods. All the spectra came from one experiment, each concentration were prepared in triplicates, resulting in a total of 21 spectra. For the sake of the readability, all spectra have been offset. B. relation between band absorbance and position of amide I determined as the position of the maximum of a 3rd order polynomial fitted to the top of amide I, between 1670 and 1630 cm-1. C. as for B. but after correction of the spectra for resonant Mie scattering with 20 iterations.[38]*

A closer look at the wells where a small quantity of cells is present shows that cells are scattered on the surface of the well resulting in abrupt changes in the refractive index. In turn, this may result in scattering effects. Visual search for negative lobes on the left hand side of amide I band of HTS spectra revealed significant dispersive artifacts as the amount of cells deposited on the well was decreasing (not shown). To further evaluate this, the relation between amide I absorbance and amide I maximum position was reported in figure 2B. The band maximum position is defined here as the position of the maximum of a 3rd order polynomial fitted to the top of amide I, between 1670 and 1630 cm^{-1}. Position is determined analytically as the root of its derivative. It must be noted that when fitting the top of the band by fitting by a third order polynomial or other band shapes, a large number of data points contribute to defining the band position, resulting in an accuracy of ca 0.1 cm^{-1}, i.e. much better than data encoding.[7,39,40] A poor reproducibility can be noticed but also a significant drift of the maximum towards higher wavenumbers as the cell number is increased. There is a clear dependence of the band position on the absorbance as Amide I maximum position shifts continuously from ca 1644 cm^{-1} to 1648 cm^{-1} when absorbance increases from 0.05 to 0.8. This observation could explain the lack of reproducibility observed if the amount of cells varies from one experiment to the next or when the cell smear is not homogenously spread. The problem is likely to be related to scattering effects due to abrupt changes in refractive indices (surface not completely covered by cells).

To test this hypothesis, the Resonant Mie scattering-EMSC algorithm of Bassan et al.[38] was applied on the HTS spectra recorded. After correction, the position of Amide I maximum shifts for all spectra from 1644 - 1648 cm^{-1} to 1654 - 1655 cm^{-1} (figure 2C). This correction had clearly more impact on 50,000 cells/well than on 400,000 cells/well HTS spectra, which indicates the importance to have enough cells on the well to avoid a large Mie Scattering artifact.

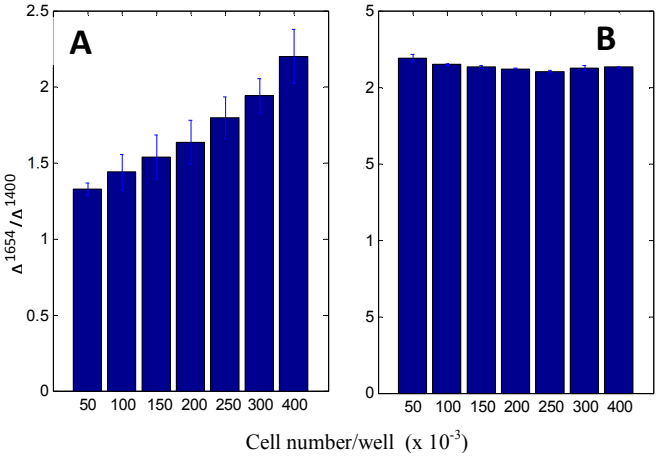

***Figure 3**: A. Evolution of the ratio of the absorbances at 1654 and 1400 cm^{-1} for the spectra described in figure 2. The number of cell per well is indicated on the abscissa. Starting from one experiment, three samples have been prepared for each cell concentration, resulting in a total of 21 spectra. Error bars report the standard deviation. B. Evolution of the ratio of absorbances after correction of the spectra for resonant Mie scattering with 20 iterations.*

A second potential issue is the one of linearity of the response. Even though in general absorbances did not exceed 1, it could happen that locally very high absorbances are present as cell smears are not homogenous, eroding the relative intensity of the most intense bands. This effect would result in variations in the intensity ratio between a strong and a weak band. Figure 3 reports the ratio of the absorbances at 1654 and 1400 cm^{-1} for the raw spectra. A quite significant evolution of this ratio can be observed (Figure 3A). Yet, it appears that this significant change largely disappears when a resonant Mie scattering correction is applied (see figure 3B) suggesting that it was due to the shift in the amide I peak maximum rather than to a real saturation effect. In conclusion, Mie scattering is an issue but saturation is not for all the conditions tested here.

Microscopic investigation of cell spectra at different cell densities

The spectra discussed so far are the mean spectra obtained on thousands of cells and provide little insight able to explain spectral properties at a microscopic level. To better understand the information contributing to the HTS spectra, FTIR images of the same cell smears were recorded using a FPA-based imaging system (Figure 4). Images have been acquired in the center of the well where cell density is rather homogenous and higher than at the edges (see Figure 1). The bright field images of 360 x 360 μm^2 located in the center of each well are presented in figure 3A for 50,000 to 300,000 cells/well deposited on the HTS ZnSe plate. The corresponding FTIR images are presented in figure 4B. They were built from the absorbance in the protein region of the spectrum (absorbance at 1654 cm^{-1}). On these IR images, the black pixels correspond to spectra that did not pass a S/N ratio of 100:1 threshold.

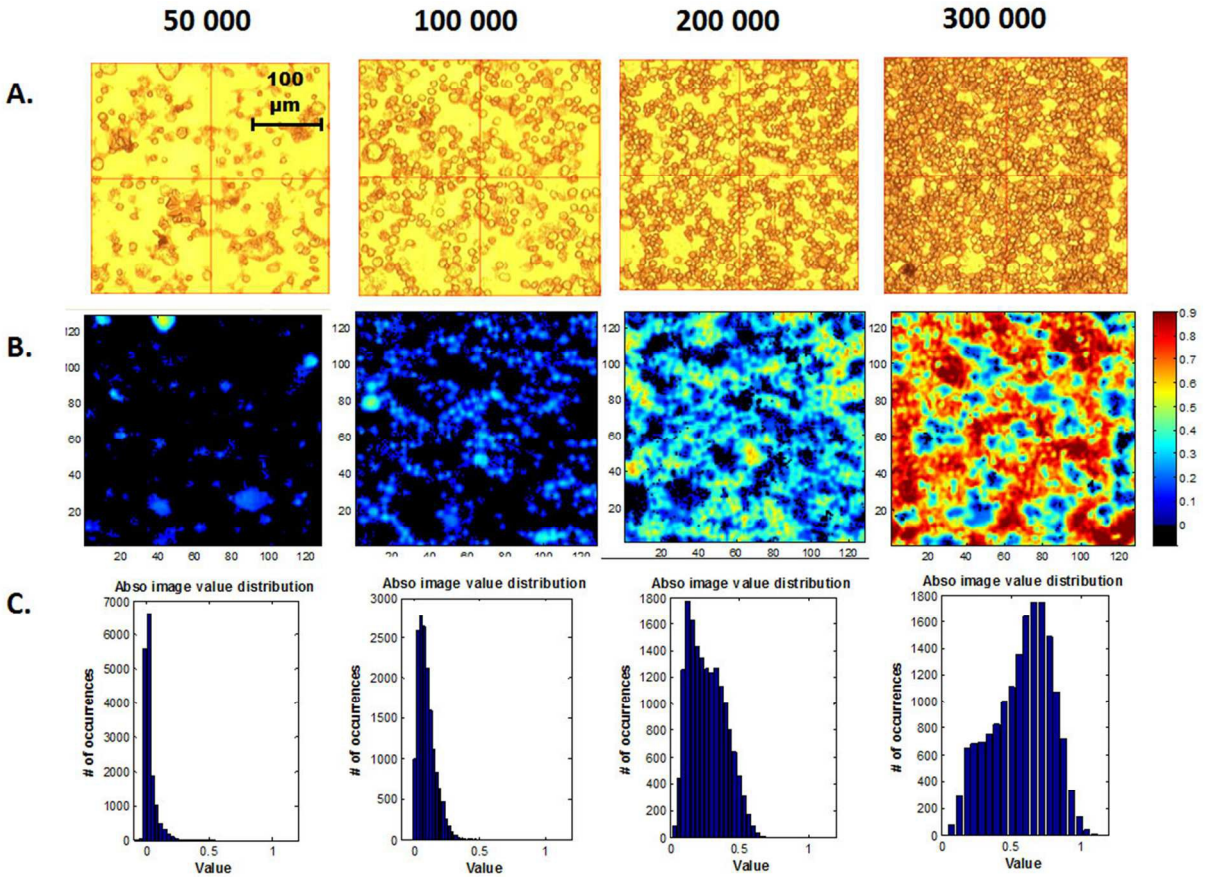

***Figure 4**: Infrared and bright field images of a 360 x 360 μm^2 image recorded in the center of a ZnSe plate well. The number of cells deposited in each well is indicated on top of the figure. **A**. 360 x 360 μm^2 bright field images of cell smears (respectively 50,000 – 100,000 – 200,000 and 300,000 cells) spread each on one well of a ZnSe plate. **B**. Corresponding FTIR images reporting the absorbance at 1654 cm^{-1}. Every black pixel corresponds to spectrum that has a S/N ratio < 100. **C**. Distribution of the absorbance values from every pixel of the images presented at B.*

The images reported in figure 4 are in reasonable agreement with the known cell size and cell number. Assuming an average diameter of 10 µm diameter for a dried MDA-MB-231 cell and considering the 6 mm diameter well, coverage should be 12,5% for 50,000 cells, 25% for 100,000 cells, 50% for 200,000 cells and 75% for 300,000 cells, more or less consistent with the microscopic view presented in Figure 4A. Analysis of the FTIR images after selecting pixels with S/N > 100 indicates a coverage of 1% for 50,000 cells/well, 6% for 100,000 cells/well, 38% for 200,000 cells/well and 84% for 300,000 cells/well. Obviously, considering the pixels with S/N>100 strongly underestimates the coverage. This is likely due to the fact that spatial resolution is limited by diffraction. At 1654 cm^{-}

[1] (ca. 6 µm), considering a numerical aperture (NA = 0.4), diffraction limits resolution to ca. 9 µm at best.[41] As the point-spread-function usually presents side lobes, true resolution is usually even further reduced in standard IR imaging.[41,42] In turn, the signal at one particular pixel is mixed with signal from neighboring pixels. When cells are isolated, neighboring pixels are empty and the absorbances get very weak. As a consequence, S/N ratio is poor.

The distribution of absorbance values at 1654 cm^{-1} for each image is represented in Figure 4C. Values of absorbance are found between 0 and 1.2, with a clear increase as the number of cells/well is increasing. For 50,000 cells, the absorbance for the majority of the spectra is close to 0, which corresponds to empty spaces. As the quantity of cells increases, empty spaces disappear, cells become contiguous and the distribution of absorbance gets wider. Interestingly, the lowest cell coverage does not provide information on the absorbance of one cell. The first predominant histogram bin contains ca 5,600 pixels for 50,000 cells/well and obviously represents empty spaces. Tentatively, it can be guessed that the second bin (absorbance between 0 and 0.025) containing ca. 6,800 pixels represents empty space close to cells where the small absorbance results from the neighboring pixels. The third bin (absorbance between 0.025 and 0.050) containing ca. 2000 pixels could be pixels belonging to cells but whose contribution is mixed with contribution from empty neighboring pixels. The next bins, representing all together ca 2,000 pixels (12.5% of the total) would originate from pixels located closer to the center of the cells. For 100,000 cells/well, the histogram culminates at an absorbance of ca 0.1 with only very few pixels with an absorbance above 0.25. When cells are more concentrated, the histogram broadens considerably, culminating at an absorbance of ca 0.7 for 300,000 cells/well. These highest absorbances are probably related to multilayers of cells.

In conclusion, the data reported in figure 4 emphasize the overlap of contributions coming from neighboring pixels and demonstrate a very broad range of absorbances. As the distribution of absorbances is not homogeneous in the wells, we could suppose that it will affect the quality of the HTS spectra, which are in fact a complex combination of spectra of variable intensities. It is therefore necessary to evaluate to which extent spectral properties vary as a function of the absorbance.

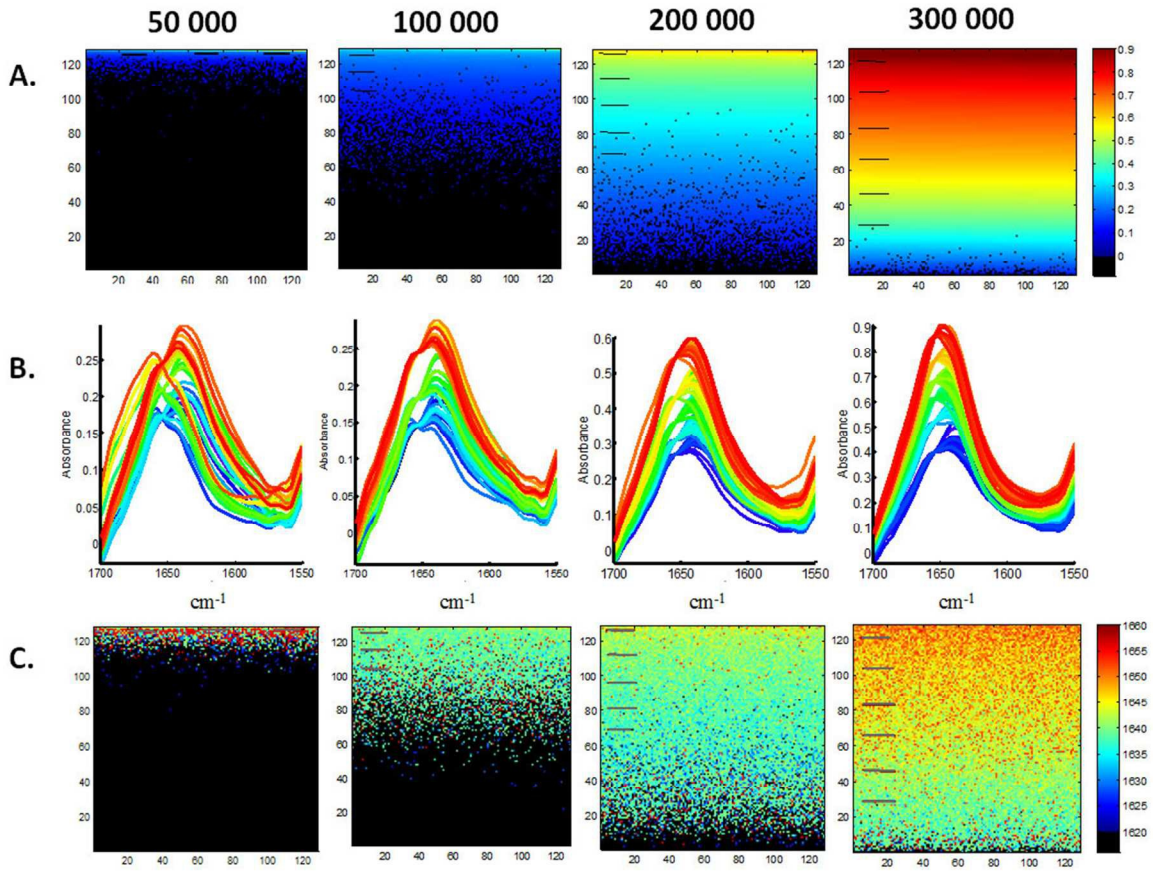

Figure 5*: Analysis of infrared images of cell smears (respectively 50,000 – 100,000 – 200,000 and 300,000 cells) spread on one well of a ZnSe plate (see Figure 4). The cell number in each well is reported on top of the figure. A. The infrared images of Figure 4B have been reworked to sort the pixels according to the absorbance at 1654 cm^{-1}. The intensity of absorbance varies between 0 and 0.9 as indicated in the right hand scale. The horizontal lines on the left hand side of each image indicate a series of ca 20 spectra of about the same absorbance at 1654 cm^{-1}. Spectra corresponding to these pixels are plotted in* ***B****. Each 20 spectrum series displays an isobestic point at 1654 cm^{-1} as they have been selected to have the same absorbance at 1654 cm^{-1}. Amide I position for each spectrum pixel presented in A is reported in* ***C****. Amide I position was determined as the position of the maximum of a 3rd order polynomial fitted to the top of amide I, between 1670 and 1630 cm^{-1}.Each image covers an area of 360 x 360 μm^2. The black pixels correspond to spectra that did not pass the S/N ratio of 100.*

Analyst RSCPublishing

ARTICLE

To evaluate this variability, the spectra of the FTIR images presented in Figure 4B were sorted according to their absorbance at 1654 cm^{-1} and new images were created with the so-sorted pixels (Figure 5A). Series of about 20 spectra of very similar absorbance (indicated by black lines on figure 5A) were extracted. The spectra corresponding to these selected pixels were plotted in figure 5B. As pixels of similar absorbance at 1654 cm^{-1} have been selected for each series, an isobestic-like point appears at 1654 cm^{-1} for each 20 spectra series. At 50,000 cells/well, only a very small fraction of the pixels with S/N>100 can be used and still present very poor reproducibility. At higher cell concentrations, a first observation is the poor reproducibility of the individual spectra. For each series of identical absorbance at 1654 cm^{-1}, there is a wide variation of the absorbance in other part of the spectra, at 1640 cm^{-1} for instance. The amide I band position was then evaluated for all spectra of Figure 5A and reported for all pixels in Figure 5C. The position of amide I peak is clearly shifting towards higher wavenumbers as the absorbance intensity increases but there is also a wide variation of band position independently of the absorbance. In conclusion, the HTS mean spectra obtained on HTS 96 well plates are the average of contributions characterized by a wide absorbance distribution and by Mie scattering effects which significantly vary from point to point. Spectrum quality is the best at the highest cell concentrations, i.e. 300,000 to 400,000 cells/well which presents the best S/N and the relatively smaller Mie scattering effect as judged from amide I band being close to 1650 cm^{-1}.

HTS-FTIR evaluation of the effect of 4 polyphenols on the MDA-MB-231 breast cancer cell line

At this point of the work, it can be safely assumed that working with 300,000 to 400,000 cells/well is the best option. Mie scattering is minimal and S/N is the highest. In order to test the potentiality of HTS spectra to identify weak spectral differences, we applied the method on MDA-MB-231 breast cancer cells exposed to four polyphenols: capsaicin, EGCG, quercetin and resveratrol. These compounds were chosen as antitumor properties have been already described for them in the literature.[43–49] In fact polyphenolic compounds are numerous and present a vast array of anticancer cellular effects.[50–54] A method for classifying their mechanism of action could be useful to help the choice of lead polyphenols for the treatment of cancer.

After treatment of the MDA-MB-231 cells with the 4 different polyphenols at their respective IC_{50} , i.e. the concentration required to inhibit 50% of the growth after 72 hours, determined using the cellular viability assay MTT [25], we recorded infrared HTS-spectra of the treated and untreated cells. All the HTS-spectra were pre-processed (water vapour subtracted, baseline corrected and normalized). Two independent experiments were realized a month apart with all the polyphenols, resulting in a total of 75 spectra (15 spectra by treatment) that were analysed as follows:

Difference spectra and Student t-test. To reveal the spectral variations induced by the different polyphenols, the mean spectra of untreated cells (controls) were subtracted from the mean spectra of treated cells. The "difference spectra" obtained represents the actual metabolic modifications induced by each polyphenol. All difference spectra were calculated with fully pre-processed spectra. Student t-test was computed at every wavenumber and results were reported on the difference spectra (polyphenol-treated minus untreated). It allowed a statistical comparison between the spectra of cells exposed to the polyphenols and control cells. Figure 6 reports the variations between the mean spectra for the data collected in the presence and absence of the different polyphenols. Wavenumbers where a significant difference occurs are indicated by black stars (significant level of $\alpha = 0.5\%$). Different spectral signatures of the effects for the 4 compounds were obtained and showed quite similar variations with respect to control spectra with more intense variations for the quercetin and EGCG compared to resveratrol and capsaicin.

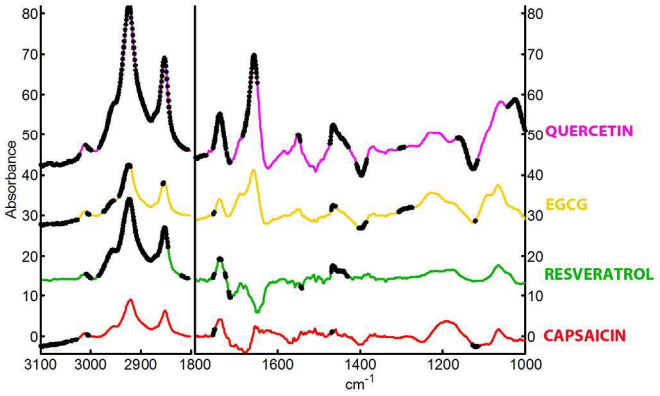

Figure 6. *Differences between mean spectra of MDA-MB-231 breast cancer cells exposed to 4 polyphenolic compounds at their respective IC_{50} and the control cells (not treated). Two independent experiments were carried with 15 samples prepared for each condition in total (treated and control) and the IR spectra were recorded, resulting in a total of 15 spectra by treatment and 75 for the entire experiment. All the HTS spectra were processed (water vapor subtracted, baseline corrected and normalized). A Student t-test was computed at every wavenumber with a significant level of $\alpha = 0.5\%$. Each black star indicates a statistically significant difference between the means.*

Principal Component Analysis. In order to observe the intrinsic proximities and distances within the data set and to group spectra according to their similarity, an unsupervised statistical analysis was achieved, the principal component analysis (PCA). It is a common statistical method used to analyse and compare FTIR spectral data. As it was observed that Mie scattering is a significant artefact that appears in HTS spectra, whether spectral reproducibility can be improved after applying a Mie scattering correction remains to be demonstrated. Therefore a PCA was applied at first on the 75 spectra only pre-processed (fig. 7A), and then on the 75 spectra pre-processed and corrected for the Mie Scattering (fig. 7B).

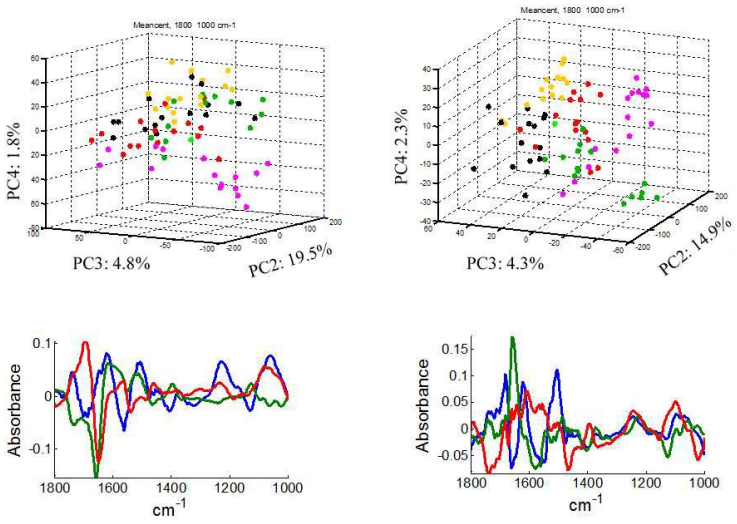

Figure 7. *Principal component analysis of 75 pre-processed and baseline corrected spectra (see Materials and Methods) from the breast cancer cell lines MDA-MB-231 exposed to 4 polyphenols at their respective IC_{50}. Top: score plots: black stars corresponds to controls, red ones to capsaicin, yellow ones to EGCG, pink ones to quercetin and green ones to resveratrol. The fraction of the variance explained is indicated on the axes. Bottom: loadings. The pre-processed spectra were used in A. and the pre-processed and resonant Mie scattering corrected spectra were used in B. The 1800-1000 cm^{-1} region was used to compute the PCA.*

Every star in each PCA plot from fig. 7 is the projection of one of the 75 HTS spectra. The different polyphenols are identified by a unique color and the controls are in black. Examination of the two PCA plots indicates that correction for resonant Mie scattering improves very significantly the clustering of spectra according to the polyphenolic treatment. Even though clustering of the spectra was improved after Mie Scattering correction, the spectra of the different treatments are still close on the PCA which might reflect quite similar effects induced by the different polyphenols and make them hard to distinguish.

Conclusions

The present paper explains to some extent the intrinsic lack of reproducibility observed for high throughput FTIR spectroscopy. It demonstrates the wide variations of absorbance distribution and Mie scattering effects at microscopic levels and suggests experimental conditions that minimize these problems. There is an ongoing debate about dispersive artifact correction, with different methods and software being used e.g references.[55–59] A theoretical issue is obviously processing mean spectra averaging various levels of scattering effects in a single way. The present study suggests that the best option is to minimize Mie scattering artefacts by deposition of enough cells to recover the entire surface of the well. Being aware of this condition to deposit the cell samples on a multi-well plate, it was applied after the treatment of a breast cancer cell line with polyphenolic compounds. Modifications induced by various polyphenols in a breast cancer cell line could be precisely recorded even if subtle differences related to the global effect of the polyphenol are more difficult to assess.

Acknowledgements

This research has been supported by grants from the National Fund for Scientific Research (FRFC 2.4533.10 and 2.4527.10, 2.4526.12 and T.0155.13). E.G. is Director of Research with the National Fund for Scientific Research (FNRS) (Belgium), A.M. is Research Fellow supported by the Fund for Research and Education within Industry and Agriculture (FRIA) from the FNRS (Belgium).

Abbreviations

HTS, High Throughput Screening; DLaTGS, Deuterated L-alanine doped TriGlycine Sulfate; EGCG, Epigallocatechin-gallate; FBS, Foetal Bovine Serum; FPA, Focal Plane Array; FTIR, Fourier Transform Infrared; IR, Infrared; MCT, Mercury Cadmium Telluride; S/N, Signal to Noise.

Notes and references

[a] Laboratory for the Structure and Function of Biological Membranes, Center for Structural Biology and Bioinformatics, Université Libre de Bruxelles (ULB), Bld du Triomphe 2, CP206/02, B-1050 Brussels, Belgium.
E-mail: egoor@ulb.ac.be; Fax: +32-2-650-53-82; Tel: +32-2-650-53-86
** Corresponding author*

References

1. M. Suggitt and M. C. Bibby, *Clin. Cancer Res.*, 2005, **11**, 971–81.
2. E. Kleiren, J. M. Ruysschaert, E. Goormaghtigh and V. Raussens, *Spectrosc. Int. J.*, 2010, **24**, 61–66.
3. H. H. de Jongh, E. Goormaghtigh, J. M. Ruysschaert and H. H. de-Jongh, *Biochemistry*, 1997, **36**, 13603–13610.
4. E. Goormaghtigh, V. Cabiaux and J. M. Ruysschaert, *Subcell.Biochem.*, 1994, **23**, 405–450.
5. E. Goormaghtigh, R. Gasper, A. Benard, A. Goldsztein, V. Raussens and A. Bénard, *Biochim Biophys.Acta-Proteins Proteomics*, 2009, **1794**, 1332–1343.
6. E. Goormaghtigh, J. M. Ruysschaert and V. Raussens, *Biophys.J.*, 2006, **90**, 2946–2957.
7. A. Derenne, T. Claessens, C. Conus and E. Goormaghtigh, in *Encyclopedia of Biophysics*, 2013, pp. 1074–1081.
8. A. Derenne, O. Vandersleyen and E. Goormaghtigh, *Biochim. Biophys. Acta*, 2013.
9. S. Boydston-White, T. Gopen, S. Houser, J. Bargonetti and M. Diem, *Biospectroscopy*, 1999, **5**, 219–27.
10. H. N. Holman, M. C. Martin, E. A. Blakely, K. Bjornstad and W. R. McKinney, *Biopolymers*, 2000, **57**, 329–335.

11. S. Boydston-White, T. Chernenko, A. Regina, M. Miljkovic, C. Matthaus and M. Diem, *Vib. Spectrosc.*, 2005, **38**, 169–177.

12. S. Boydston-White, M. Romeo, T. Chernenko, A. Regina, M. Miljkovic and M. Diem, *Biochim. Biophys. Acta-Biomembranes*, 2006, **1758**, 908–914.

13. K. R. Flower, I. Khalifa, P. Bassan, D. Démoulin, E. Jackson, N. P. Lockyer, A. T. McGown, P. Miles, L. Vaccari and P. Gardner, *Analyst*, 2011, **136**, 498–507.

14. C. Hughes, M. D. Brown, F. J. Ball, G. Monjardez, N. W. Clarke, K. R. Flower and P. Gardner, *Analyst*, 2012, **137**, 5736–42.

15. A. Derenne, A. Mignolet and E. Goormaghtigh, *Analyst*, 2013, **138**, 3998–4005.

16. R. Gasper and E. Goormaghtigh, *Analyst*, 2010, **135**, 3048–3051.

17. M. Verdonck, N. Wald, J. Janssis, P. Yan, C. Meyer, A. Legat, D. E. Speiser, C. Desmedt, D. Larsimont, C. Sotiriou and E. Goormaghtigh, *Breast cancer and melanoma cell line identification by FTIR imaging after formalin-fixation and paraffin-embedding.*, 2013, vol. 138.

18. F. Draux, P. Jeannesson, C. Gobinet, J. Sule-Suso, J. Pijanka, C. Sandt, P. Dumas, M. Manfait and G. D. Sockalingum, *Anal. Bioanal. Chem.*, 2009, **395**, 2293–2301.

19. G. Berger, R. Gasper, D. Lamoral-Theys, A. Wellner, M. Gelbcke, R. Gust, J. Neve, R. Kiss, E. Goormaghtigh, F. Dufrasne and J. Nève, *Int. J. Oncol.*, 2010, **37**, 679–686.

20. R. Gasper, T. Mijatovic, R. Kiss and E. Goormaghtigh, *Spectrosc. Int. J.*, 2010, **24**, 45–49.

21. R. Gasper, T. Mijatovic, A. Bénard, A. Derenne, R. Kiss, E. Goormaghtigh and A. Benard, *Biochim. Biophys. Acta - Mol. Basis Dis.*, 2010, **1802**, 1087–1094.

22. R. Gasper, G. Vandenbussche and E. Goormaghtigh, *Biochim Biophys Acta*, 2011, **1808**, 597–605.

23. R. Gasper, T. Mijatovic, R. Kiss and E. Goormaghtigh, *Appl. Spectrosc.*, 2011, **65**, 584–594.

24. A. Derenne, V. Van Hemelryck, D. Lamoral-Theys, R. Kiss and E. Goormaghtigh, *Biochim. Biophys. Acta*, 2012, **1832**, 46–56.

25. A. Derenne, R. Gasper and E. Goormaghtigh, *Analyst*, 2011, **136**, 1134–1141.

26. A. Derenne, M. Verdonck and E. Goormaghtigh, *Analyst*, 2012, **137**, 3255–64.

27. R. Gasper, J. Dewelle, R. Kiss, T. Mijatovic and E. Goormaghtigh, *Biochim. Biophys. Acta - Biomembr.*, 2009, **1788**, 1263–1270.

28. D. Naumann, D. Helm and H. Labischinski, *Nature*, 1991, **351**, 81–82.

29. A. Bosch, A. Minan, C. Vescina, J. Degrossi, B. Gatti, P. Montanaro, M. Messina, M. Franco, C. Vay, J. Schmitt, D. Naumann and O. Yantorno, *J.Clin.Microbiol.*, 2008, **46**, 4118.

30. D. Naumann, V. Fijala, H. Labischinski and P. Giesbrecht, *J. Mol. Struct.*, 1988, **174**, 165–170.

31. D. Helm, H. Labischinski and D. Naumann, *J. Microbiol. Methods*, 1991, **14**, 127–142.

32. P. Szymański, M. Markowicz and E. Mikiciuk-Olasik, *Int. J. Mol. Sci.*, 2012, **13**, 427–52.

33. J. Major, *J. Biomol. Screen.*, 1998, **3**, 13–17.

34. J. Ollesch, M. Heinze, H. M. Heise, T. Behrens, T. Brüning and K. Gerwert, *J. Biophotonics*, 2014, **7**, 210–21.

35. E. Goormaghtigh, in *Adv. Biomed. Spectrosc. (Biological and Biomedical Infrared Spectroscopy)*, eds. A. Barth and P.I.Haris, IOS Press, 2009, vol. IOS Press, pp. 104–128.

36. E. Goormaghtigh, in *Encyclopedia of Biophysics*, 2013, pp. 1074–1081.

37. E. Goormaghtigh and J. M. Ruysschaert, *Spectrochim.Acta*, 1994, **50A**, 2137–2144.

38. P. Bassan, A. Kohler, H. Martens, J. Lee, H. J. Byrne, P. Dumas, E. Gazi, M. Brown, N. Clarke and P. Gardner, *Analyst*, 2010, **135**, 268–277.

39. B. Szalontai, Y. Nishiyama, Z. Gombos and N. Murata, *Biochim. Biophys. Acta*, 2000, **1509**, 409–19.

40. R. Mendelsohn, M. A. Davies, J. W. Brauner, H. F. Schuster and R. A. Dluhy, *Biochemistry*, 1989, **28**, 8934–8939.

41. P. Lasch and D. Naumann, *Biochim. Biophys. Acta*, 2006, **1758**, 814–29.

42. E. C. Mattson, M. J. Nasse, M. Rak, K. M. Gough and C. J. Hirschmugl, *Anal. Chem.*, 2012, **84**, 6173–80.

43. N. H. Thoennissen, J. O'Kelly, D. Lu, G. B. Iwanski, D. T. La, S. Abbassi, A. Leiter, B. Karlan, R. Mehta and H. P. Koeffler, *Oncogene*, 2010, **29**, 285–96.

44. G. Galati and P. J. O'Brien, *Free Radic. Biol. Med.*, 2004, **37**, 287–303.

45. J. Kanwar, M. Taskeen, I. Mohammad, C. Huo, T. H. Chan and Q. P. Dou, *Front. Biosci. (Elite Ed).*, 2012, **4**, 111–31.

46. E. C. Stuart, M. J. Scandlyn and R. J. Rosengren, *Life Sci.*, 2006, **79**, 2329–36.

47. X.-H. Deng, H.-Y. Song, Y.-F. Zhou, G.-Y. Yuan and F.-J. Zheng, *Exp. Ther. Med.*, 2013, **6**, 1155–1158.

48. J. Duo, G.-G. Ying, G.-W. Wang and L. Zhang, *Mol. Med. Rep.*, 2012, **5**, 1453–6.

49. S. He, C. Sun and Y. Pan, *Int. J. Mol. Sci.*, 2008, **9**, 842–53.

50. G. G. Duthie, S. J. Duthie and J. a Kyle, *Nutr. Res. Rev.*, 2000, **13**, 79–106.

51. J. D. Lambert, J. Hong, G. Yang, J. Liao and C. S. Yang, *Am. J. Clin. Nutr.*, 2005, **81**, 284–291.

52. K. W. Lee and H. J. Lee, *Biofactors*, 2006, **26**, 105–21.

53. S. Ramos, *J. Nutr. Biochem.*, 2007, **18**, 427–42.

54. S. Ramos, *Mol. Nutr. Food Res.*, 2008, **52**, 507–26.

55. P. Bassan, A. Kohler, H. Martens, J. Lee, E. Jackson, N. Lockyer, P. Dumas, M. Brown, N. Clarke and P. Gardner, *J. Biophotonics*, 2010, **3**, 609–20.

56. P. Bassan, A. Sachdeva, A. Kohler, C. Hughes, A. Henderson, J. Boyle, J. H. Shanks, M. Brown, N. W. Clarke and P. Gardner, *Analyst*, 2012, **137**, 1370–7.

57. B. Bird, M. Miljković and M. Diem, *J. Biophotonics*, 2010, **3**, 597–608.

58. K. R. Bambery, B. R. Wood and D. McNaughton, *Analyst*, 2012, **137**, 126–32.

59. A. Dazzi, A. Deniset-Besseau and P. Lasch, *Analyst*, 2013, **138**, 4191–201.

Infrared spectra of cell smear change shape with cell density